

## Effects of Build Parameters on the Mechanical and Di-Electrical Properties of AM parts

Sai Sri Nidhi Munaganuru<sup>1\*</sup>, Muthu Ram Prabhu Elenchezhian<sup>1</sup>, Vamsee Vadlamudi<sup>1</sup>,  
Rauhon Ahmed Shaik<sup>1</sup>, Hari Kishore Adluru<sup>2</sup>, Md Rassel Raihan<sup>3</sup> and Kenneth Reifsnider<sup>4</sup>

<sup>1</sup>Graduate Students, Department of Mechanical and Aerospace Engineering,  
The University of Texas at Arlington, Arlington, TX 76019

<sup>2</sup>Postdoctoral Research Fellow, Institute for Predictive Performance Methodologies,  
The University of Texas at Arlington Research Institute, Fort Worth TX 76118

<sup>3</sup>Research Scientist, Institute for Predictive Performance Methodologies,  
The University of Texas at Arlington Research Institute, Fort Worth TX 76118

<sup>4</sup>Presidential Distinguished Professor, Department of Mechanical and Aerospace Engineering,  
The University of Texas at Arlington, Arlington, TX 76019

\*Corresponding Author: [saisrinidhi.munaganuru@mavs.uta.edu](mailto:saisrinidhi.munaganuru@mavs.uta.edu)

### Abstract

Additive manufacturing (AM) revolutionized many industries, i.e., Automotive, Biomedical, Aerospace and Defense. As opposed to traditional manufacturing methods, a part is manufactured layer by layer from 3D CAD models in AM. Though the vision of AM is impressive, there are many challenges that are hindering the widespread use of these complex parts. One of the challenges in these materials is defects grow and their orientation during the manufacturing process. In this paper we are going to investigate the effect of Build Parameters and their effects on the mechanical and electrical properties of the additively manufactured heterogeneous material system. We will study the electrical properties to find out the material state of additively manufactured part.

### Introduction

Additive manufacturing(AM), a formal term for Rapid Prototyping(RP) is used in a variety of industries to describe a process for rapidly creating a system or part representation before final release or commercialization. In other words, the emphasis is on creating something quickly and that the output is a prototype or basis model from which further models and eventually the final product will be derived [1]. There are a variety of individual processes which differ in their method of layer manufacturing. Individual processes will differ depending on the material and machine technology used. Material extrusion is one of the most common and commercial method used for Additive Manufacturing. The printer that was used for this paper follows the principle of ‘Fused Deposition Modelling(FDM)’. This approach extrudes the material through a nozzle in a controlled manner. FDM uses a heating chamber to liquefy polymer that is fed into the system as a filament. The filament is pushed into the chamber by a tractor wheel arrangement and it is this pushing that generates the extrusion pressure as shown in Figure 1. The main drawback to using this technology is the build speed. The inertia of the plotting heads means that the maximum speeds and accelerations that can be obtained are somewhat smaller than other systems. Furthermore, FDM requires material to be plotted in a point-wise, vector fashion that involves many changes in direction. [1]

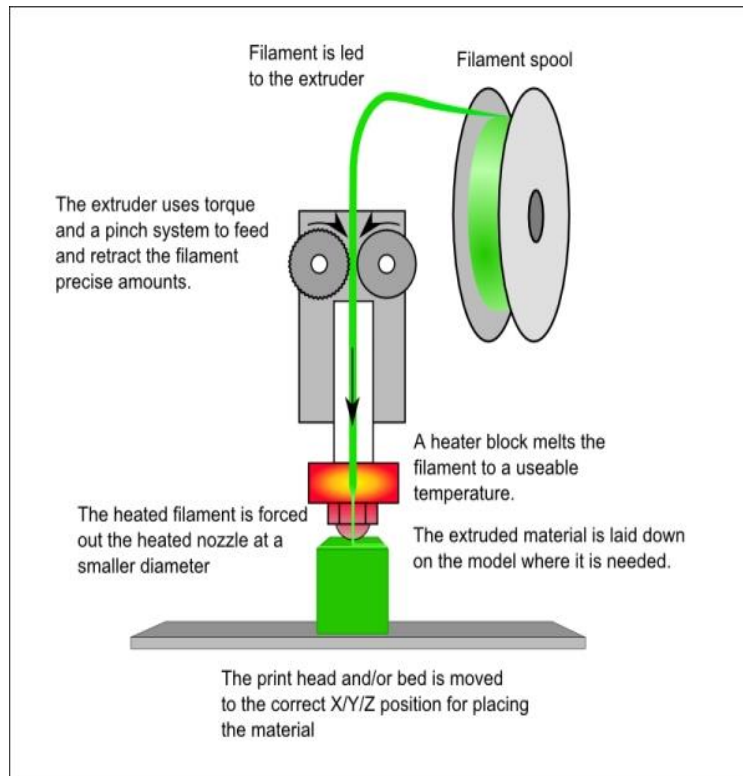


Figure 1 :- Fused Deposition Molding [2]

For practical applications, these 3D-printed parts must tolerate significant amounts of mechanical, thermal, environmental etc. loads and hence it is of great importance to determine the required strengths, and at the very least, the physical properties of these 3D-printed parts should be comparable to those manufactured by conventional methods [3]. Due to the nature of the process that builds the parts layer by layer, the mechanical properties of the part depend on the material used and processing parameters which include the raster orientation, extrusion temperature, bed temperature, infill percentage, patterns and many others. For the following study, bed temperature and infill percentage are chosen as variables to determine their effect on the material performance. To characterize these materials, mechanical and dielectric tests (using Broadband dielectric spectroscopy (BbDS) are performed on the printed parts.

BbDS is a well- established tool for dielectric material characterization which has been used in polymer industries for a long time, e.g., in composite manufacturing this method is used to monitor the curing process. A material system is comprised of multiple polarization mechanisms such as ionic (molecular), dipolar (orientational), electronic, interfacial (Maxwell–Wagner–Sillars) polarization and hopping charge polarization. The following Figure 2 shows the different types of polarization and their effect on the dielectric response and its corresponding effective frequency range. BbDS is the interaction of electromagnetic waves with matter in the frequency range from a lower value of  $10^{-6}$  Hz to a higher frequency of  $10^{12}$  Hz. This dynamic range contains information about the molecular and collective dipolar fluctuation; charge transport and polarization effects occur at inner and outer boundaries in the form of different dielectric properties of the material under study [4].

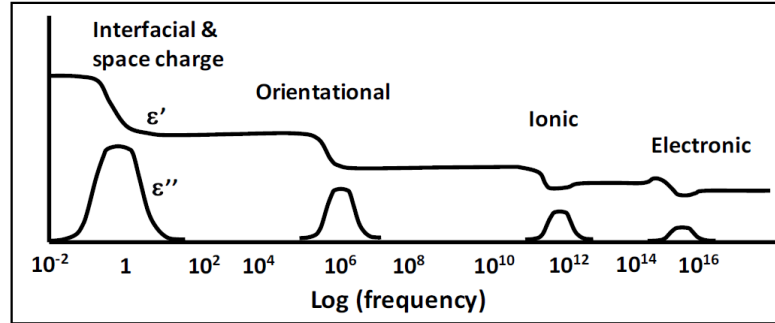


Figure 2:- Effect of different charge displacement mechanisms on dielectric response and their corresponding effective frequency range

Polar molecules are contained inside of heterogeneous materials and in the presence of an applied electric field it will polarize the material by orienting the dipole moments of polar molecules and charge accumulation at the interfaces of dissimilar materials. The polarization of a linear dielectric is given as:

$$P = \epsilon_0 \chi E \quad (1)$$

here,  $\chi$  = tensor of dielectric susceptibility

$\epsilon_0$  = dielectric permittivity of vacuum i.e.,  $8.854 \times 10^{-12}$  F/m

$E$  = Electric Field.

Now, based on Maxwell's laws of electromagnetism, we have the equation,

$$\nabla \cdot D = \rho \quad (2)$$

This is also known as Gauss Law, Where,  $\nabla \cdot$  = Divergence operator,  $D$  = Electric Displacement Field and  $\rho$  = Electric charge volume density

The relation between the dielectric displacement and electric field is given as

$$D = \epsilon_0 E + P \quad (3)$$

From (1),

$$D = \epsilon_0 E + \epsilon_0 \chi E \quad (4)$$

$$D = \epsilon_0 \epsilon_r E \quad (5)$$

In this case,  $\epsilon_r = (1 + \chi)$  is known as relative permittivity. Finally, we get  $D = \epsilon E$  where  $\epsilon = \epsilon_0 \epsilon_r = \epsilon' - \epsilon''$  is defined as complex permittivity in which  $\epsilon'$  is the real part of the complex permittivity and  $\epsilon''$  is the imaginary part, in other words the dielectric loss. Thus, we can now plot two graphs, one for the real part of the permittivity and other for the imaginary part, both of which corresponds to the logarithmic values of the frequencies.

The schematic of the setup is shown below in Figure 3. The arrangement is like a parallel plate capacitor, where in one end of the electrode an alternating signal is supplied and the other end of the electrode is grounded.

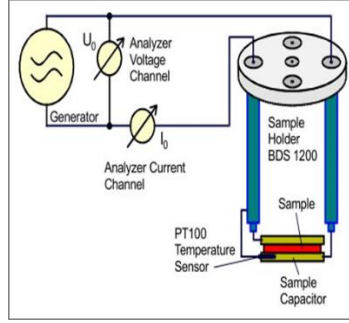


Figure 3:- Schematic of the dielectric response setup

An AC voltage can be represented by equation 6.

$$U(t) = U_0 \cos(\omega t) = \text{Re}(U^* \exp(i\omega t)) \quad (6)$$

Where  $U^* = U_0$ , is the amplitude of the signal applied,  $\omega$  is the frequency of the applied signal. The measured current can be represented by equation 7.

$$I(t) = I_0 \cos(\omega t + \varphi) = \text{Re}(I^* \exp(i\omega t)) \quad (7)$$

$$I^* = I' + iI'' \quad (8)$$

$$I_0 = \sqrt{I'^2 + I''^2} \quad (9)$$

$$\tan(\varphi) = \frac{I''}{I'} \quad (10)$$

$$Z^* = Z' + iZ'' = \frac{U^*}{I^*} \quad (11)$$

Where  $I'$  is the real part of measured current,  $I''$  is the imaginary part of measured current,  $\varphi$  is the measured phase lag,  $Z'$  is the measured real impedance of the material system,  $Z''$  is the imaginary part of impedance of the material system and the complex permittivity can be calculated by

$$\varepsilon^*(\omega) = \varepsilon' - i\varepsilon'' = \frac{-i}{\omega Z^*(\omega)} \cdot \frac{1}{C_0} \quad (12)$$

Where  $C_0$  is the capacity of the empty sample capacitor.

Recently BbDS has been used by several researchers [5-7] to characterize composite materials and were able to study the relation of dielectric properties to material performance. Raihan et, al. [6] used Dielectric Relaxation Strength (DRS) which is the algebraic difference

between static permittivity value and the limiting frequency permittivity value as shown below in (13) to characterize the material.

$$\Delta\epsilon = \epsilon_s - \epsilon_\infty \quad (13)$$

Higher DRS indicates more interfacial polarization owing to charge accumulation around boundaries (voids, cracks etc.), indicating a lower mechanical strength.

### **Design of Experiments**

In the current study, the infill percentage and bed temperature were considered independent variables and the mechanical strength properties – peak force, stiffness, ultimate tensile strength (UTS) and dielectric property DRS are considered dependent variables. Table I shows different values considered for infill percentages and bed temperatures for the study. For each case, 3 specimens were used to take in to consideration the statistics of each case.

*Table I Tabulated values of various infill percentages and bed temperatures*

Infill Percentage (%)	12.5	33	50	100
Bed-Temperature(°C)	50	75	80	

### **Specimen Preparation and Material Selection**

#### **Design**

A 3D CAD model was designed using SolidWorks. For mechanical testing the samples were designed following the ASTM D638 [8] Type-1 standards as shown in Figure 4(a) with 7mm thickness and for dielectric testing circular samples of 40mm width with a thickness of 7mm were printed. The nature of the process leads to creation of rough surface because of which the electrode contact is not uniform with the sample surface. In order to improve the contact, two surfaces were marked 25x25mm square on either sides and two-part silver epoxy (working time 10 minutes and curing time 48 hours) was uniformly spread in these squares as shown in Figure 4(b).

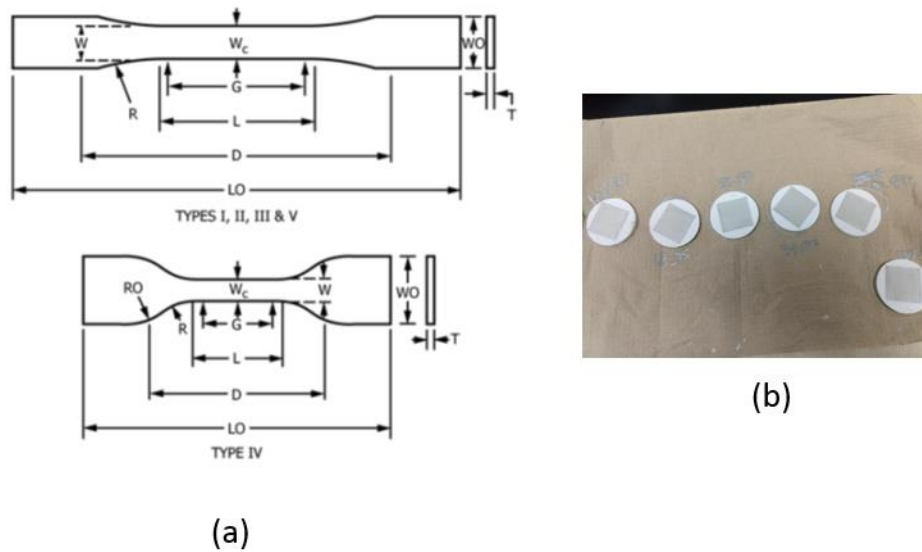


Figure 4:- (a) Coupons for mechanical testing (b) Circular Specimens for dielectric testing

## **Material**

Polylactic acid, one of the most common FDM materials is used for the current study. The greatest advantages for PLA in FDM printing are the facts that it creates no toxic gases while melting and so can be printed with no ventilation system, and it has low glass transition temperature. Table II shows the tabulated values of various properties of PLA available in literature.

Table II Tabulated values of various properties of PLA available in literature [9]

Property (units)	Value
Extrude temperature (°C)	180-220
Bed temperature (°C)	20-55
CTE ( $\mu\text{m}/\text{m}\cdot^\circ\text{C}$ )	85
$T_g$ (°C)	60-65
Tensile Modulus (MPa)	2.7-16

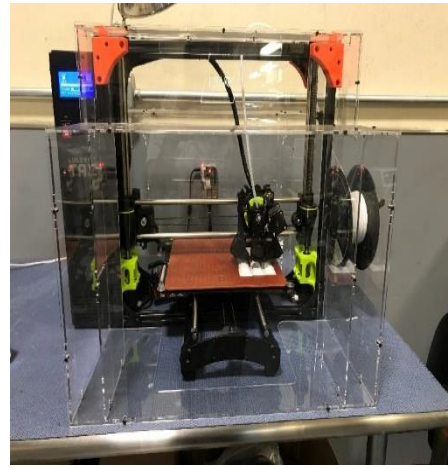
## **Experimental Setup**

### **3D Printer Setup**

The samples were printed using Lulzbot Taz at UTARI. The printer functions with Fused Deposition modeling along with an automatic Bed Levelling System up to a Maximum Bed Temperature of 120°C (248°F). It has a print area of 280 mm x 280 mm x 250 mm (11.02 in x 11.02 in x 9.8 in) with a maximum Print Speed of 200 mm/sec (7.9 in/sec) and an average Print Speed of 30 - 50 mm/sec (1.18 - 1.97in/sec). It can be used to print with a variety of materials like, PLA, ABS, PVA, HIPS, Polyester (Tritan), PETT, bronze etc. Figure 5 shows the printer setup and samples which are being printed.



(a)



(b)

Figure 5:- Specimen Preparation using Lulzbot Taz printer at UTARI

### Dielectric Testing Setup

An in-house manufactured faraday cage was used to block out external interferences. The broadband dielectric/impedance spectrometer, manufactured by Novocontrol<sup>®</sup>, was used for carrying out the dielectric study. The sample was placed between two copper electrodes of 0.5-inch diameter embedded in blocks made of polycarbonate material. A voltage of 1.0 V is applied to the sample resulting in a flow of current with a phase shift. The dielectric properties of the material system are calculated using equations 10-12. Figure 6 shows the equipment setup that was used to carry out the experiments.

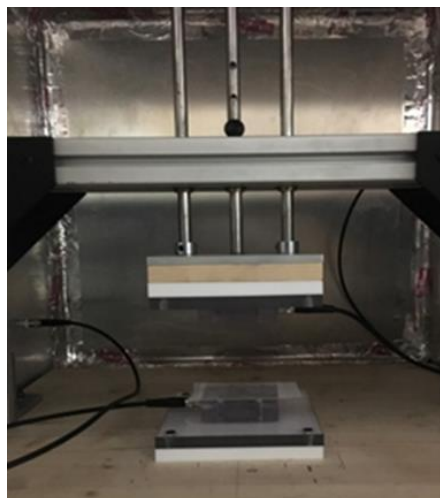


Figure 6:- Dielectric Testing setup

## Mechanical Testing Setup

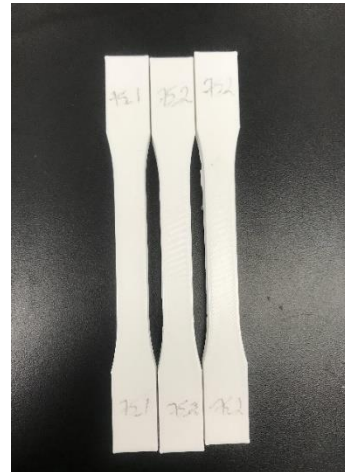
Axial Tension test was performed on the MTS<sup>®</sup> tensile testing machine equipped with 50 KN load cell and hydraulic wedge grips at IPPM UTARI. The gripping pressure was approximately 12.5-150 psi (based on infill percentage) as shown in Table III. Static axial tensile loading was applied using displacement control at a constant rate of  $0.025\text{mm}\cdot\text{s}^{-1}$ . The testing setup and a set of samples used for testing are shown in Figure 7.

Table III MTS Testing Grip Pressures based on Infill Percentage

Infill Percentage (%)	Grip Pressure(psi)
12.5%	12.5
33%	50
50%	100
100%	150



(a)



(b)

Figure 7:- (a) MTS setup and (b) Set of specimens used for testing

## Results & Discussion

A series of tensile tests were conducted on a set of AM fabricated samples with varying process parameters. Figure 8 shows the fractured set of specimens.



Figure 8:- Fractured set of specimens after mechanical testing

The observed mechanical and dielectric properties are tabulated below in

Table IV. The ultimate tensile strength (UTS) and DRS values along with the coefficient of variation of the mechanical test data for each set is shown below. The axial displacement and axial force from the MTS test for various infill percentages at 50 °C bed temperature are shown in Figure 9.

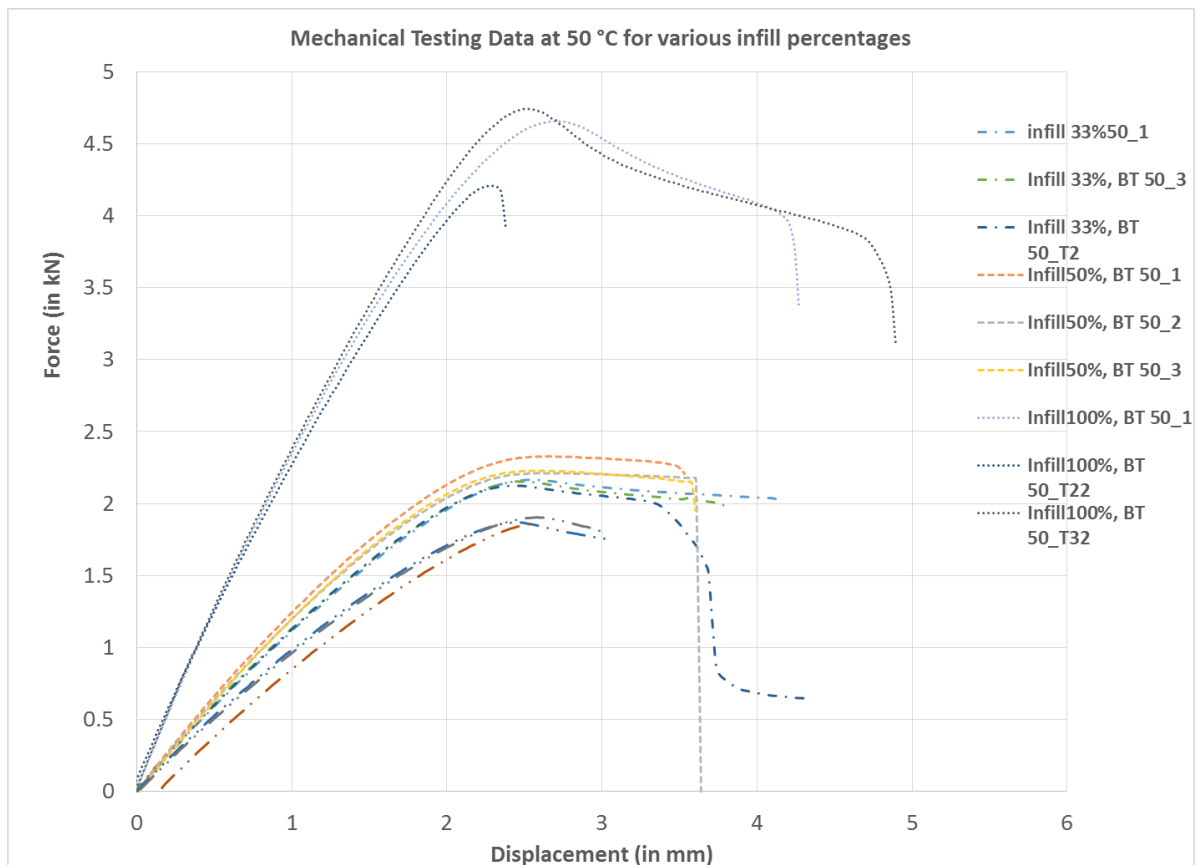


Figure 9 Force-Displacement plots at 50 °C for various infill percentages

Table IV Tabulated results of Mechanical and dielectric testing

Set	Infill %	Bed Temp (°C)	UTS (MPa)	DRS	% CV
1	12.5	50	20.62	0.04	1.285
2		75	20.63	0.102	1.73
3		80	20.034	0.038	1.59
4	33	50	23.627	0.05	1.005
5		75	23.136	0.02	1.63
6		80	22.8	0.03	1.563
7	50	50	26.203	0.05	2.77
8		75	26.02	0.03	1.3
9		80	24.78	0.033	1.36
10	100	50	49.833	0.16	2.21
11		75	48.62	0.03	6.31439

### **Discussion**

From table IV, for 12.5 % infill set 2 (75°C bed temperature) specimens exhibited highest DRS values and had highest strength. This may be a result of material inflow across the voids due to high bed temperature. This additional material tends to reduce the internal residual stresses which ultimately increases the strength of the specimen. The permittivity as a function of frequency for various infills at different bed temperatures are shown in Figure 10.

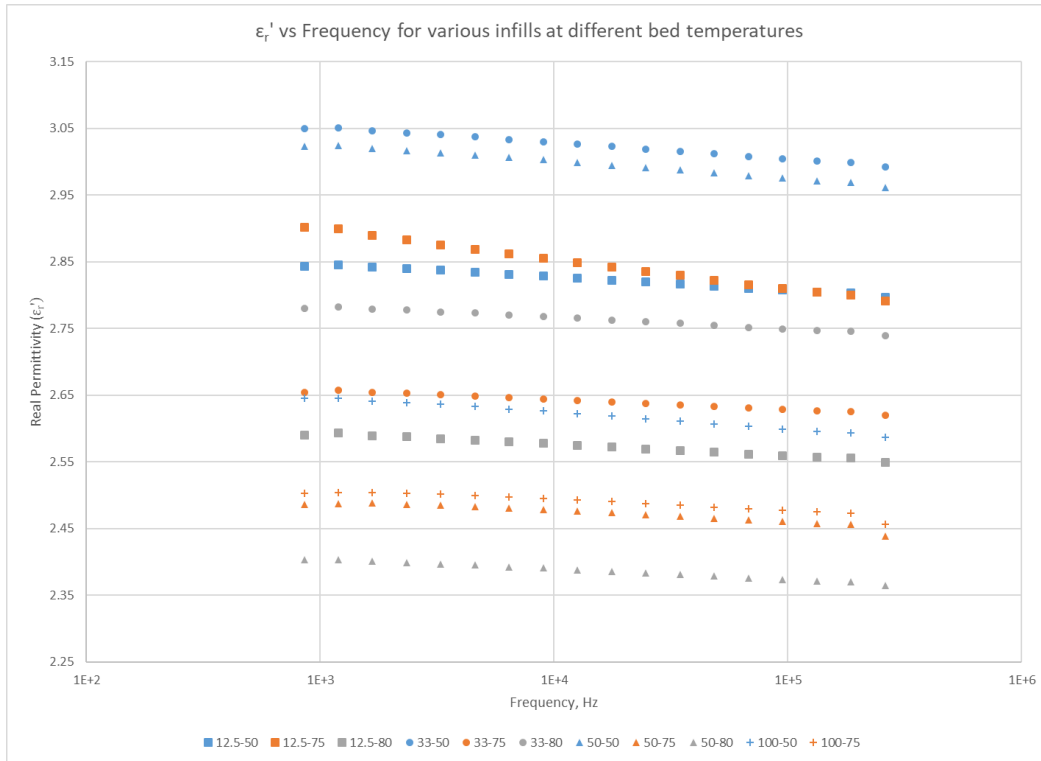


Figure 10:- Variation of real permittivity with frequency for various infill's at different bed temperatures

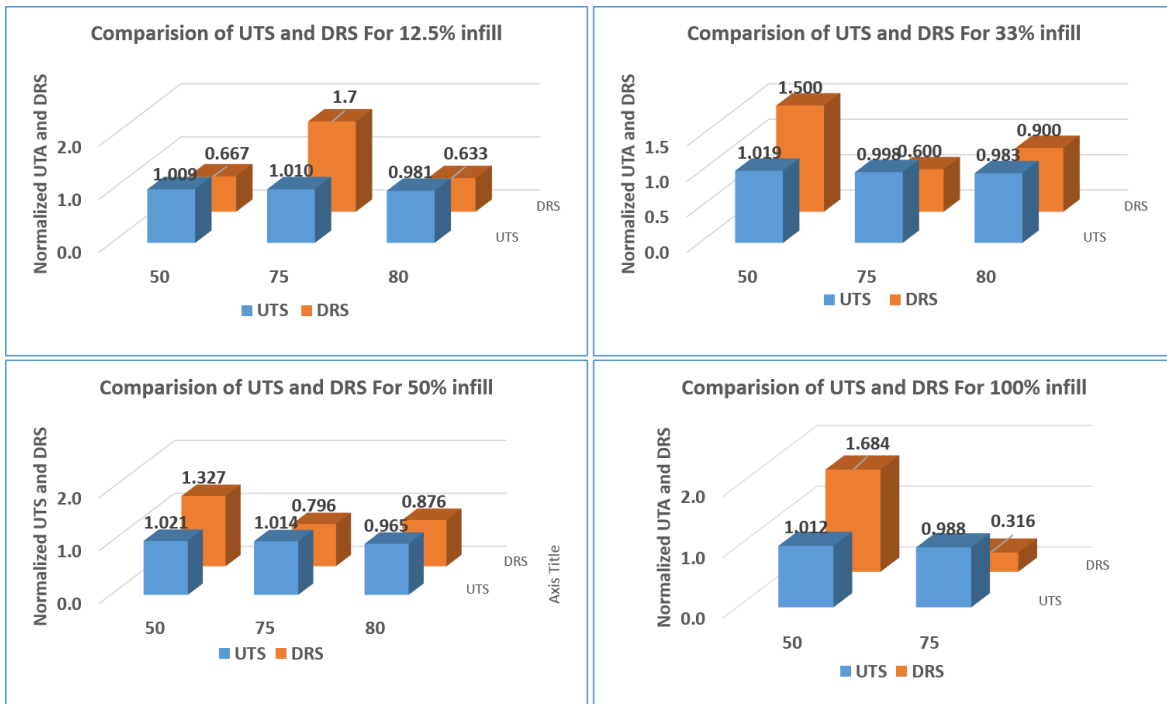


Figure 11:- Comparison of mechanical and dielectric characterization for various infill's at different bed temperatures

From Figure 11, it can be observed that higher the DRS value, higher the ultimate tensile strength (UTS) in most of the cases with some discrepancies for 33 % and 50 % infill. This contradicts the observations made for polymer matrix composites by Raihan et.al. [5] which had different phases with different conductivity and permittivity where as these 3D printed coupons have only PLA filaments. This needs further analysis and will be published in subsequent journal publication

### **Conclusion and Future Work**

In this work the influence of two independent build parameters on FDM manufactured specimens was investigated using mechanical and dielectric characterization of 3D printed samples. The investigated material was Polylactic acid (PLA). In most cases studied, higher DRS value corresponded to higher strength. It was observed that 50 °C bed temperature had the highest DRS and strength in most cases as it is lower than the glass transition temperature of the material system (60-65 °C), whereas the other bed temperatures used in the study (75,80 °C) are higher.

Further investigation is required before a concrete conclusion can be made on the pattern observed here. The authors are exploring other parameters such as Infill shape, Raster Orientation, nozzle temperature, other Materials etc.

### **Acknowledgement**

The authors would like to thank David Manivanh-Equipment Technician and all the staff and interns at the Institute of Predictive Performance Methodologies of the University of Texas at Arlington Research Institute, for providing support with the equipment and testing towards this work.

### **References**

1. Gibson I., Rosen D., Stucker B. (2015). *Additive Manufacturing Technologies*. Springer, New York, NY
2. Stokes, M. B. (2013). *3D Printing for Architects with MakerBot*. Packt Publishing Ltd.
3. Dizon, J. R. C., Espera, A. H., Chen, Q., & Advincula, R. C. (2017). Mechanical characterization of 3D-printed polymers. *Additive Manufacturing*.
4. Schönhals A., Kremer F. (2003). *Broadband Dielectric Spectroscopy*. Springer, Berlin, Heidelberg
5. Banerjee, P. K., Elenchezian, M. R. P., Vadlamudi, V., Raihan, R., & Reifsnider, K. (2017). Predicting Adhesive Bond Performance Based on Initial Dielectric Properties. *Proceedings American Society for Composites*.
6. Raihan, R., Adkins, J. M., Baker, J., Rabbi, F., & Reifsnider, K. (2014). Relationship of dielectric property change to composite material state degradation. *Composites Science and Technology*, 105, 160-165.
7. Reifsnider, K., Raihan, M. R., & Vadlamudi, V. (2016). Heterogeneous fracture mechanics for multi-defect analysis. *Composite Structures*, 156, 20-28.
8. ASTM International. (2014). *ASTM D638-14 Standard Test Method for Tensile Properties of Plastics*. Retrieved from <https://doi.org/10.1520/D0638-14>
9. Bates, G.K., Howie, T. (2017). *Materials for 3D Printing by Fused Deposition*. Retrieved from [http://www.materialseducation.org/educators/matedu-modules/docs/Materials\\_in\\_FDM.pdf](http://www.materialseducation.org/educators/matedu-modules/docs/Materials_in_FDM.pdf)